Nanoscale Advances

ROYAL SOCIETY OF CHEMISTRY

COMMUNICATION

View Article Online
View Journal | View Issue

Cite this: *Nanoscale Adv.*, 2024, **6**, 792

Received 24th November 2023
Accepted 9th January 2024

DOI: 10.1039/d3na01041d

rsc.li/nanoscale-advances

Polymer removal and dispersion exchange of (10,5) chiral carbon nanotubes with enhanced 1.5 μm photoluminescence†

Yahui Li,[ab] Ye Liu,[b] Feng Jin,[b] Leitao Cao,[b] Hehua Jin,[ab] Song Qiu *[ab] and Qingwen Li *[a]

Singe-chirality single-walled carbon nanotubes (SWCNTs) produced by selective polymer extraction have been actively investigated for their semiconductor applications. However, to fulfil the needs of biocompatible applications, the organic solvents in polymer-sorted SWCNTs impose a limitation. In this study, we developed a novel strategy for organic-to-aqueous phase exchange, which involves thoroughly removing polymers from the sorted SWCNTs, followed by surfactant covering and redispersing of the cleaned SWCNTs in water. Importantly, the obtained aqueous system allows us to perform sp^3 functionalization of the SWCNTs, leading to a strong photoluminescence emission at 1550 nm from the defect sites of (10,5) SWCNTs. These functionalized SWCNTs as infrared light emitters show considerable potential for bioimaging applications. This exchange-and-functionalization strategy opens the door for future biocompatible applications of polymer-sorted SWCNTs.

Introduction

Semiconducting single-walled carbon nanotubes (s-SWCNTs) have immense potential in various fields such as high-performance field-effect transistors,[1,2] radiofrequency devices,[3] optoelectronic devices,[4] quantum photonics,[5] and biological imaging[6] due to their unique optoelectronic properties. Currently, solution-processed separation methods based on either organic or aqueous phases show promise in the development of applications of s-SWCNTs. Among the methods, polymer sorting in the organic phase exhibits advantages in obtaining high semiconductor purity, and advantages in fabricating high-quality thin-film devices which have demonstrated performance surpassing that of silicon-based transistors at equivalent dimensions.[7,8] Meanwhile, aqueous-phase separation methods facilitate the SWCNT applications that require biocompatibility, such as in biological imaging,[9] drug delivery,[10] biosensing,[11] and gene detection.[12]

Single-chirality SWCNTs as near-infrared second window bioimaging and single-photon emitter materials require more chiral species emitting in the telecommunication wavelength range. Currently, aqueous phase separation methods can achieve batch-wise sorting of chiral species below 1.1 nm.[13–15] However, for larger diameter SWCNTs, the chiral selectivity decreases. SWCNTs obtained through polymer-based separation can effectively fill the gaps in certain emission regions.[16] The chemical functionalization of SWCNTs is another factor that needs to be considered for light emission applications. sp^3 functionalization reactions can introduce rich functional groups in water solutions, allowing tunable movement of the fluorescence emission peak to the optical communication C-band. Although organic-phase functionalization reactions have been developed, the efficiency of defect introduction still needs further improvement, and the achievement of fluorescence emission in the optical communication C-band has not been realized.[17] Currently, the optimal performance of single-chirality SWCNT single-photon emitters is achieved through efficient functionalization reactions in water.[18] Therefore, the future applications of SWCNTs in specific areas will require SWCNT solutions in different solvent systems. To fully exploit the advantages of SWCNTs in both organic and aqueous systems, solvent exchange after polymer separation is necessary. However, this aspect is currently seldom investigated.

For the removal of polymers, many methods have been reported including polymer cleaning in solution,[19] polymer degradation,[20–22] the rinsing of thin films,[23] cleaning after introducing coatings,[24,25] and annealing treatments.[26] However, these methods are still challenging to integrate into the solvent exchange process. Bao *et al.* proposed a polymer removal method based on flocculation,[27] but the polymer cleaning efficiency is limited, and SWCNTs can only be maintained in

[a]*School of Nano-Tech and Nano-Bionics, University of Science and Technology of China, 96 Jinzhai Road, Hefei 230026, China. E-mail: sqiu2010@sinano.ac.cn; qwli2007@sinano.ac.cn*

[b]*Division of Advanced Nano-Materials, Suzhou Institute of Nanotech and Nano-bionics, Chinese Academy of Science, 398 Ruoshui Road, Suzhou 215123, China*

† Electronic supplementary information (ESI) available. See DOI: https://doi.org/10.1039/d3na01041d

a dispersed state in organic solvents. Niβler *et al.* developed an electrophoretic exchange purification method.[28] It requires the introduction of a complex process involving a salt layer phase and is only effective for small-diameter (6,5) species in solvent exchange. To exchange the dispersion from the organic to aqueous phase, two key issues need to be overcome simultaneously. Firstly, both the free polymer in the dispersion and the polymer coated on the SWCNT surfaces must be removed as much as possible. Secondly, SWCNTs remain loosely agglomerated rather than tightly bundled until they are redispersed in a surfactant-containing aqueous solution. At the current stage, established exchange methods generally have low efficacy, causing a high loss of SWCNTs.

In this study, we developed a solvent exchange strategy to transfer HiPCO s-SWCNTs and (10,5) SWCNTs from the organic phase into a surfactant-containing aqueous solution. This approach leverages the advantages of the high semiconductor purity and the large diameters of polymer-sorted SWCNTs, broadening the application of SWCNTs in scenarios that require biocompatibility. Based on this method, we presented sp^3 functionalization of polymer sorted s-SWCNTs in an aqueous solution, showing that (10,5) SWCNTs can emit brighter light at 1550 nm – a wavelength corresponding to the optical communication C-band.

Results and discussion

To achieve the dispersion exchange of SWCNTs from the organic to the aqueous phase, HiPCO raw SWCNT materials and two conjugated polymers, poly[(9,9-dioctylfluorenyl-2,7-diyl)-*alt*-(1,4-benzo-{2,1′-3}-thiadiazole)] (F8BT) and 9-(1-octanoyl)-9*H*-carbazole-2,7-dial (PCZ), were employed for the separation of s-SWCNTs and (10,5) single-chirality SWCNTs (Fig. S1†). These distinct organic-phase SWCNT dispersions served as the initial materials for the subsequent phase transfer process. For detailed procedures see the Experimental section. As illustrated in Fig. 1, the challenge in phase exchange lies in the strong π–π interactions between carbon nanotubes and surface polymers which make it difficult for surfactants to have space to form stable micelles on the surface and disperse in an aqueous solution.[29] Hence, the primary objective is the removal of polymer coatings from the SWCNT surface.

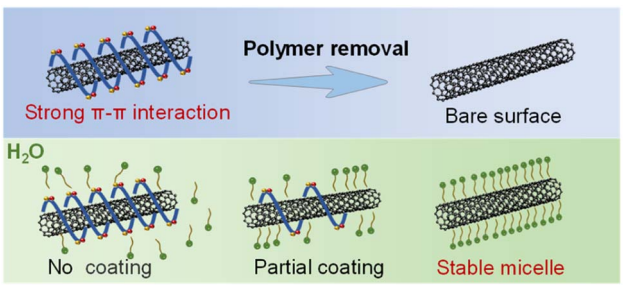

Fig. 1 Schematic diagram of polymer-wrapped carbon nanotubes and surfactant-coated carbon nanotubes. In an aqueous solution, the complete removal of wrapped polymers is crucial for the formation of stable surfactant micelles on the surface of carbon nanotubes.

Fig. 2a illustrates the partial steps of the polymer cleaning process. Firstly, the removal of most free polymers from the solution is necessary. Vacuum filtration followed by washing the filter cake with tetrahydrofuran (THF) is a commonly used method as reported previously.[19] However, this method becomes insufficient for removing polymers coated on the surface because simple solvent rinsing cannot break the van der Waals forces between carbon nanotubes and polymers. Trifluoroacetic acid (TFA) can protonate the carbon nanotubes, introducing more positive charges that disrupt the balance of π–π interactions, causing the polymers to detach from the surface of SWCNTs. However, the actual result is that once some polymers detach, carbon nanotubes with exposed surfaces tend to aggregate more easily, leading them to be directly centrifuged. Therefore, a single wash with TFA is far from adequate. In this work, we gradually detached surface polymers through multiple re-dispersion steps and the addition of TFA until a small amount of surface-coated polymer could no longer allow carbon nanotubes to be redispersed in toluene. Fig. 2b shows the absorption of polymers and carbon nanotubes in the redispersion solution after sequential cleaning, while Fig. 2c displays the filtered solution and the supernatant after centrifugation, both indicating the gradual removal of polymers. The polymer cleaning results for HiPCO s-SWCNTs are presented in Fig. S2.†

Once the redispersion in toluene became impractical, chloroform was employed as the redispersion solvent. Due to the higher polarity, chloroform exhibited better dissolving capacity for SWCNTs, and only fewer polymers on the surface of SWCNTs are needed to maintain solution stability. TFA was reintroduced to facilitate the detachment of a small number of remaining polymers from the surface of SWCNTs (Fig. 3a). The final redispersion was achieved in an aqueous solution

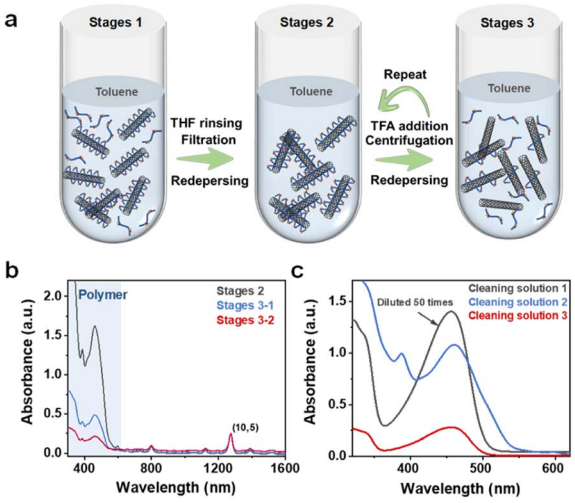

Fig. 2 (a) Schematic diagram of polymer removal in toluene solvent. (b) The absorption spectra of (10,5) SWCNTs after redispersion in toluene solvent after one round of THF rinsing and two rounds of TFA rinsing. (c) The absorption spectra of the filtrate and the supernatant after three cleaning cycles. In (b) and (c), the legend texts share colours with their corresponding plots.

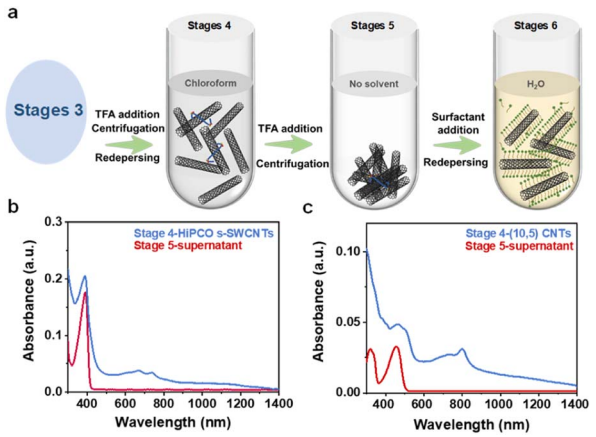

Fig. 3 (a) Schematic diagram of polymer removal in chloroform solvent and deionized water. (b) The absorption spectra of SWCNTs with (10,5) tubes as the dominant chiral species and supernatant. (c) The absorption spectra of SWCNTs with (10,5) tubes as the dominant chiral species in toluene and H_2O. In (b) and (c), the legend texts share colours with their corresponding plots.

containing surfactants. The key to the entire process lies in two points: firstly, consistently keeping nanotubes dissolved while continuously washing off surface-coated polymers, and secondly, employing a centrifugal force of only 2000*g* at each step ensure that SWCNTs remain in a loose state and do not readily aggregate into stronger bundles. Fig. 3b and c display the absorption spectra of polymers and SWCNTs in chloroform. Due to the solvent effect of chloroform, the absorption peaks of carbon nanotubes are no longer visible, but the polymer peaks

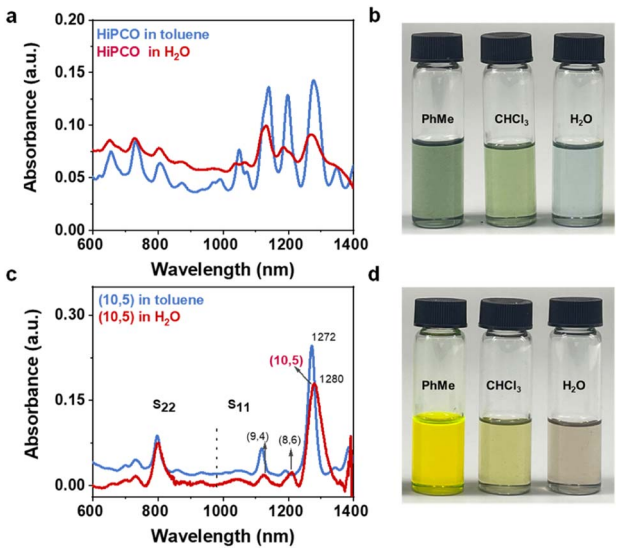

Fig. 4 (a) The absorption spectra of HiPCO s-SWCNTs in toluene and H_2O. (b) Optical photographs of HiPCO s-SWCNTs in toluene (PhMe), chloroform ($CHCl_3$), and aqueous solutions. (c) The absorption spectra of SWCNTs with (10,5) tubes as the dominant chiral species in toluene and H_2O. (d) Optical photographs of SWCNTs with (10,5) tubes as the dominant chiral species in toluene (PhMe), chloroform ($CHCl_3$), and aqueous solutions. In (a) and (c), the legend texts share colours with their corresponding plots.

are discernible. Therefore, the difference in the absorbance of polymer peaks represents the trace amount of residual polymer on the surface of SWCNTs. At these polymer concentrations, HiPCO s-SWCNTs and (10,5) SWCNTs can be re-dispersed in an aqueous solution with the aid of surfactants. Through calculations, it was found that the removal efficiency of the polymer is >99.9% (Fig. S3†). Fig. 4a compares the absorption spectra of HiPCO s-SWCNTs in polymer and aqueous solution. The s-SWCNTs are completely transferred to the aqueous solution, while the absorption peaks of metallic carbon nanotubes are entirely invisible (Fig. S4†). Fig. 4b shows a photograph of HiPCO s-SWCNT solutions at different stages of solvent exchange. This illustrates the advantage of polymer separation in obtaining high-purity s-SWCNTs, with the potential for further broadening the application prospects of solution-based SWCNT separation through aqueous phase exchange. Fig. 4c shows the absorption spectra that contain (10,5) species as the dominant products, and contain a few (8,6) and (9,4) species. Fig. 4d shows a photograph of (10,5) SWCNT solutions at different stages of solvent exchange. We calculated a yield of approximately 60% from the initial dispersion of SWCNTs to aqueous solution according to the optical absorbance (Fig. S5†).[6] This is because the cleaning process of toluene and chloroform completely collects SWCNT precipitates at every step. Only the final step of centrifugation in aqueous solution requires the removal of some nanotubes that are not stably coated by surfactants. To further improve the yield of solvent exchange, choosing more suitable solvents or chemical substances to make the polymer more easily fall off the surface of nanotubes may be an efficient strategy. After the system exchange, the S_{11} absorption peak of (10,5) species exhibits a broadened profile in the aqueous phase, accompanied by an 8 nm redshift in the peak position (Fig. 4c). This may be because the E_{11} transition is affected by the dielectric constant of different solvents and the dispersants with different spatial configurations.[30] Based on this, we have successfully utilized the designed universal solvent exchange strategy to transfer s-SWCNTs and single-chirality SWCNTs from the organic phase to the aqueous dispersion system. Meanwhile, considering the decreased separation efficiency of the aqueous phase separation system for SWCNTs with diameters larger than 1 nm,[31] solvent exchange from the organic phase to aqueous solution is meaningful for the preparation of large diameter single-chirality SWCNTs in the future. The advantage of this solvent exchange strategy is that SWCNTs do not undergo strong annealing, repeated filtration[19] and strong centrifugation during polymer removal,[16] so they can remain relatively loose and not easily form tight bundles, being easily redispersed in a new solvent.[28] Moreover, this strategy does not introduce too many defects and has a higher yield. On the other hand, the shortcoming is that the strategy contains many steps. In the future, it is expected that more suitable solvents or chemical substances will be chosen to make the polymer more easily fall off the surface of nanotubes, so as to reduce the experimental steps.

After obtaining aqueous dispersions of two different types of SWCNTs, we attempted to introduce sp^3 defects on the surface

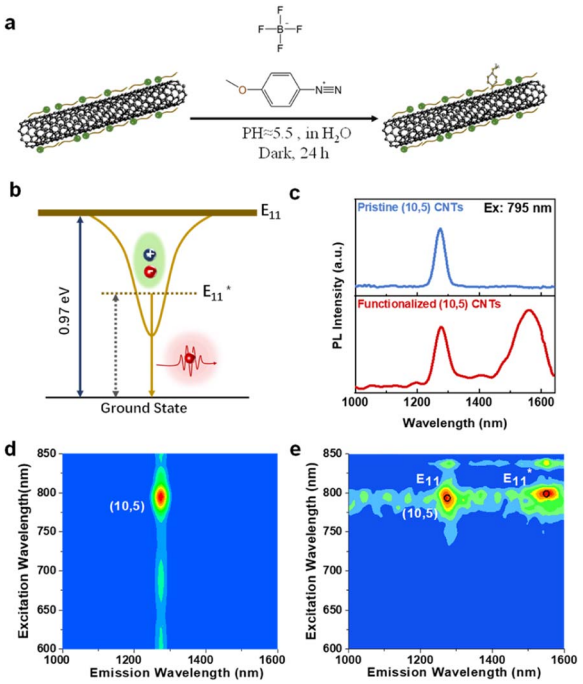

Fig. 5 (a) Reaction formula of carbon nanotubes and 4-methoxybenzenediazonium tetrafluoroborate. (b) Band diagrams of (10,5) SWCNTs with sp^3 defects. (c) Photoluminescence emission spectra of (10,5) SWCNTs before and after introducing sp^3 defects. (d) and (e) show the photoluminescence excitation–emission mapping of (10,5) SWCNTs before and after introducing sp^3 defects.

of SWCNTs using the most employed functionalization reaction in aqueous solutions. The reaction involved mixing a solution of 4-methoxybenzenediazonium tetrafluoroborate with a solution of SWCNTs, followed by a simple reaction in the dark to obtain functionalized SWCNTs (Fig. 5a). The detailed process is provided in the Experimental section.

For HiPCO s-SWCNTs, we used an excitation wavelength of 725 nm to detect the photoluminescence (PL) spectra of the solution before and after the reaction under the same test conditions. The PL spectra in Fig. S6a† show that the original spectrum had the strongest emission peak at 1284 nm, with the overall emission mainly occurring before the wavelength of 1400 nm. However, the PL spectrum after functionalization shows a redshift of the strongest emission wavelength to 1345 nm, and the emission intensity in the range of 1000–1100 nm has almost disappeared. This indicates that SWCNTs originally located in this region have been sufficiently introduced with sp^3 defects, resulting in an overall redshift. The emission intensity after 1400 nm significantly increased and extended to around 1550 nm. The photoluminescence excitation–emission (PLE) maps in Fig. S6b and c† further validate these results. We propose that the introduction of sp^3 defects in SWCNTs in HiPCO SWCNTs leads to an overall redshift, and the reason 1345 nm becomes the strongest PL emission peak is due to the redshift of the fluorescence of smaller-diameter carbon nanotubes and the insufficient reaction of SWCNTs originally located in this region. The superposition of the PL signals of these two aspects ultimately results in 1345 nm being the strongest PL peak after the functionalization of HiPCO s-SWCNTs.

Single-chirality SWCNTs offer a clearer demonstration of their bandgap tuning capabilities in the presence of sp^3 defects. We conducted functionalization reactions on (10,5) SWCNTs to mitigate the impact of multi-chirality on fluorescence emission signals. Fig. 5b illustrates the band diagram of (10,5) species with sp^3 defects. sp^3 defects introduce a deep trap state E_{11}* below the original E_{11} (0.97 eV) of the carbon nanotube, where optically generated excitons are captured and can relax to the ground state, emitting a single photon at a lower energy. This results in a redshift of the peak position and potentially higher emission intensity in the fluorescence spectrum. Previous reports suggest that SWCNTs can be tuned by introducing different functional groups to control the redshift of the deep trap state E_{11}*, achieving effective matching of the final telecommunications wavelengths (1.0 to 1.55 μm).[32] In this study, Fig. 5c shows the PL spectra where the introduction of 4-methoxybenzene shifts the original E_{11} emission peak at 1276 nm to the E_{11}* emission peak at 1557 nm, satisfying the zero-loss window at 1550 nm in the optical communication C-band. The normalized PL spectrum reveals a higher emission intensity at 1550 nm compared to 1276 nm. Organic-phase functionalization reactions reported so far have not achieved fluorescence emission in this wavelength range. Table 1 summarizes the peak parameters in E_{11} and E_{11}* before and after functionalization. The introduction of sp^3 defects in (10,5) species results in a 175 meV shift in the E_{11} peak position and a significant increase in the full width at half maximum (FWHM). PLE maps in Fig. 5d and e further validate these results, but the functionalization reaction retains the fluorescence emission intensity of (10,5) SWCNTs. We speculate that the larger diameter exacerbates the steric hindrance effect of chemical reactions, thereby increasing the difficulty of the reaction. Nevertheless, the redshift to 1550 nm and its higher emission intensity has significant implications for carbon nanotubes as single-photon source materials in quantum information applications. The efficient results of functionalization reactions on (10,5) SWCNTs after the exchange from the organic to the aqueous phase also confirm the importance of

Table 1 E_{11} and E_{11}* peak parameters of (10,5) SWCNTs with sp^3 defects

	Pristine		Covalently functionalized				
(n,m)	E_{11}	FWHM	E_{11}	FWHM	E_{11}*	FWHM	E_{11}* − E_{11}
(10,5)	1275 nm	37 nm	1276 nm	51 nm	1557 nm	98 nm	175 meV

solvent exchange strategies for expanding the photonic applications of SWCNTs in the future.

Conclusion

In summary, we achieved the exchange of organic-phase solvents to an aqueous solution in a straightforward manner using simple centrifugation and redispersion methods employed during the SWCNT solution-based separation method. Building on this foundation, sp^3 functionalization was efficiently carried out in an aqueous solution. Ultimately, the intrinsic emission peak of (10,5) species at 1276 nm was shifted to 1557 nm in the optical communication C-band. This lays a solid material groundwork for future applications, including near-infrared fluorescence bioimaging and single-photon sources for quantum devices, utilizing single-chirality SWCNTs. The prospect of a simple and efficient organic to aqueous phase exchange strategy holds the potential to further broaden the biocompatible application prospects of SWCNTs.

Author contributions

Q.-W. L. and S. Q. conceived the idea and supervised the project. Y.-H. L. conducted most of the experiments, characterization and data analysis. Y.-H. L. and S. Q. wrote the paper. All authors discussed the results and contributed to manuscript preparation.

Conflicts of interest

The authors declare no competing financial interest.

Acknowledgements

This research was generously supported by the National Key Research and Development Program of China (2020YFA0714700) and the National Natural Science Foundation of China (22075312).

References

1 A. Javey, J. Guo, Q. Wang, M. Lundstrom and H. Dai, *Nature*, 2003, **424**(6949), 654–657.
2 Y. Lin, Y. Cao, S. Ding, P. Zhang, L. Xu, C. Liu, Q. Hu, C. Jin, L.-M. Peng and Z. Zhang, *Nat. Electron.*, 2023, **6**(7), 506–515.
3 H. Shi, L. Ding, D. Zhong, J. Han, L. Liu, L. Xu, P. Sun, H. Wang, J. Zhou, L. Fang, Z. Zhang and L.-M. Peng, *Nat. Electron.*, 2021, **4**(6), 405–415.
4 Y. Liu, S. Wang and L. M. Peng, *Adv. Energy Mater.*, 2016, **6**(17), 1600522.
5 X. He, H. Htoon, S. K. Doorn, W. H. P. Pernice, F. Pyatkov, R. Krupke, A. Jeantet, Y. Chassagneux and C. Voisin, *Nat. Mater.*, 2018, **17**(8), 663–670.
6 Y. Yomogida, T. Tanaka, M. Zhang, M. Yudasaka, X. Wei and H. Kataura, *Nat. Commun.*, 2016, **7**, 12056.
7 G. J. Brady, A. J. Way, N. S. Safron, H. T. Evensen, P. Gopalan and M. S. Arnold, *Sci. Adv.*, 2016, **2**(9), e1601240.
8 L. Liu, J. Han, L. Xu, J. Zhou, C. Zhao, S. Ding, H. Shi, M. Xiao, L. Ding, Z. Ma, C. Jin, Z. Zhang and L.-M. Peng, *Science*, 2020, **368**(6493), 850–856.
9 S. Diao, G. Hong, J. T. Robinson, L. Jiao, A. L. Antaris, J. Z. Wu, C. L. Choi and H. Dai, *J. Am. Chem. Soc.*, 2012, **134**(41), 16971–16974.
10 A. Razzazan, F. Atyabi, B. Kazemi and R. Dinarvand, *Mater. Sci. Eng., C*, 2016, **62**, 614–625.
11 J. Ackermann, J. T. Metternich, S. Herbertz and S. Kruss, *Angew. Chem., Int. Ed. Engl.*, 2022, **61**(18), e202112372.
12 J. Bornholdt, A. T. Saber, B. Lilje, M. Boyd, M. Jorgensen, Y. Chen, M. Vitezic, N. R. Jacobsen, S. S. Poulsen, T. Berthing, S. Bressendorff, K. Vitting-Seerup, R. Andersson, K. S. Hougaard, C. L. Yauk, S. Halappanavar, H. Wallin, U. Vogel and A. Sandelin, *ACS Nano*, 2017, **11**(4), 3597–3613.
13 G. Ao, J. K. Streit, J. A. Fagan and M. Zheng, *J. Am. Chem. Soc.*, 2016, **138**(51), 16677–16685.
14 J. Wang, Y. Zhou, Z. Wang, A. Rasmita, J. Yang, X. Li, H. J. von Bardeleben and W. Gao, *Nat. Commun.*, 2018, **9**(1), 4106.
15 D. Yang, L. Li, X. Wei, Y. Wang, W. Zhou, H. Kataura, S. Xie and H. Liu, *Sci. Adv.*, 2021, **7**(8), eabe0084.
16 Y. Li, M. Zheng, J. Yao, W. Gong, Y. Li, J. Tang, S. Feng, R. Han, Q. Sui, S. Qiu, L. Kang, H. Jin, D. Sun and Q. Li, *Adv. Funct. Mater.*, 2022, **32**(1), 2107119.
17 S. Settele, F. J. Berger, S. Lindenthal, S. Zhao, A. A. El Yumin, N. F. Zorn, A. Asyuda, M. Zharnikov, A. Hogele and J. Zaumseil, *Nat. Commun.*, 2021, **12**(1), 2119.
18 X. He, N. F. Hartmann, X. Ma, Y. Kim, R. Ihly, J. L. Blackburn, W. Gao, J. Kono, Y. Yomogida, A. Hirano, T. Tanaka, H. Kataura, H. Htoon and S. K. Doorn, *Nat. Photonics*, 2017, **11**(9), 577–582.
19 X. Yu, D. Liu, L. Kang, Y. Yang, X. Zhang, Q. Lv, S. Qiu, H. Jin, Q. Song, J. Zhang and Q. Li, *ACS Appl. Mater. Interfaces*, 2017, **9**(18), 15719–15726.
20 T. Lei, X. Chen, G. Pitner, H. S. Wong and Z. Bao, *J. Am. Chem. Soc.*, 2016, **138**(3), 802–805.
21 Q. Ji, J. Han, X. Yu, S. Qiu, H. Jin, D. Zhang and Q. Li, *Carbon*, 2016, **105**, 448–453.
22 J. Han, Q. Ji, H. Li, G. Li, S. Qiu, H. B. Li, Q. Zhang, H. Jin, Q. Li and J. Zhang, *Chem. Commun.*, 2016, **52**(49), 7683–7686.
23 G. J. Brady, Y. Joo, M.-Y. Wu, M. J. Shea, P. Gopalan and M. S. Arnold, *ACS Nano*, 2014, **8**(11), 11614–11621.
24 Z. Ma, J. Han, S. Yao, S. Wang and L. M. Peng, *ACS Appl. Mater. Interfaces*, 2019, **11**(12), 11736–11742.
25 G. Hills, C. Lau, A. Wright, S. Fuller, M. D. Bishop, T. Srimani, P. Kanhaiya, R. Ho, A. Amer, Y. Stein, D. Murphy, Arvind, A. Chandrakasan and M. M. Shulaker, *Nature*, 2019, **572**(7771), 595–602.
26 D. Zhong, Z. Zhang, L. Ding, J. Han, M. Xiao, J. Si, L. Xu, C. Qiu and L.-M. Peng, *Nat. Electron.*, 2017, **1**(1), 40–45.

27 T. Z. Gao, T. Lei, F. Molina-Lopez and Z. Bao, *Small Methods*, 2018, **2**(10), 1800189.
28 R. Nissler, F. A. Mann, H. Preiss, G. Selvaggio, N. Herrmann and S. Kruss, *Nanoscale*, 2019, **11**(23), 11159–11166.
29 L. Vaisman, H. D. Wagner and G. Marom, *Adv. Colloid Interface Sci.*, 2006, **128–130**, 37–46.
30 A. Dzienia, D. Just and D. Janas, *Nanoscale*, 2023, **15**(21), 9510–9524.
31 Y. Chen, M. Lyu, Z. Zhang, F. Yang and Y. Li, *ACS Cent. Sci.*, 2022, **8**(11), 1490–1505.
32 A. H. Brozena, M. Kim, L. R. Powell and Y. Wang, *Nat. Rev. Chem.*, 2019, **3**(6), 375–392.